Raman scattering of atoms from a quasicondensate in a perturbative regime

T. Wasak,[1] J. Chwedeńczuk,[1] P. Ziń,[2,3] and M. Trippenbach[1]
[1]*Faculty of Physics, University of Warsaw, ul. Hoża 69, 00-681 Warszawa, Poland*
[2]*Narodowe Centrum Badań Jądrowych, ul. Hoża 69, 00-681 Warszawa, Poland*
[3]*Université Paris Sud, CNRS, LPTMS, UMR 8626, Orsay 91405, France*
(Received 5 March 2012; revised manuscript received 6 September 2012; published 22 October 2012)

Using the perturbative approach, it is demonstrated that the widths of the density and second-order correlation function of atoms scattered from a quasicondensate in a Raman process are sensitive to the phase fluctuations induced by the nonzero temperature of the mother cloud. It is also shown how these widths evolve during expansion of the halo of scattered atoms. It is also argued that if the Raman scattering is preceded by expansion of the mother cloud, the density of atoms widens substantially, while the second-order correlation function remains practically unchanged. These results are useful for planning future Raman scattering experiments and indicate the degree of spatial resolution of atom-position measurements necessary to detect the temperature dependence of the quasicondensate. All the calculations are performed using experimental parameters of a metastable ^{4}He* quasicondensate of the Palaiseau group.

DOI: 10.1103/PhysRevA.86.043621 PACS number(s): 67.85.−d, 03.75.Nt, 42.50.Nn, 42.50.Ct

I. INTRODUCTION

Atoms scattered out of Bose-Einstein condensates can be objects of benchmark tests of various quantum mechanical models. A prominent example is a collision of two counterpropagating condensates [1–8]. During the collision, which takes place at supersonic velocity, atoms are scattered into initially empty modes, and description of such a process requires fully quantum treatment. This can be done semianalytically in the Bogoliubov approximation [9–13] or numerically in more general cases [14–18]. The analysis reveals strong correlations between the scattered atoms [4,10–13] and sub-Poissonian fluctuations of the opposite-momentum atom counts [6]. Therefore, the many-body atomic states created in the collisions could have potential application for ultraprecise sub-shot-noise atomic interferometry [19].

A different relevant example of atom scattering out of a coherent cloud takes place in a spin-1 condensate [20–22]. In this case, a single stationary matter wave is prepared in a Zeeman substate with $m_F = 0$. A two-body interaction can change the spin projection of the colliding pair into $m_F = \pm 1$. Recently, it has been demonstrated [22] that the produced atomic pairs are usefully entangled from an atom-interferometry point of view.

Here we concentrate on another pair production process, namely the Raman scattering [23,24]. In this case, an ultracold atomic cloud is illuminated with a strong laser beam. As a result, an interatomic transition leads to creation of a correlated Stokes photon and atomic excitation. The scattered pairs are correlated analogously to those produced in the condensate- or spin-changing collisions. Raman scattering is similar to the elastic Rayleigh process [25,26], though the Stokes photons have different energies than the incident light. This process has been widely studied theoretically [27–31] and observed experimentally in ultracold samples [32] and Bose-Einstein condensates [33–36]. In this work we consider a different source of Raman-scattered particles, namely the quasicondensate, which forms in strongly elongated traps [37–40]. Due to the nonzero temperature of the gas, phase fluctuations occur and they limit the spatial coherence of the system. This, as we argue below, has influence on the Raman process and alters both the density and the second-order correlation function of the scattered atoms.

The paper is organized as follows. In Sec. II we formulate the three-dimensional problem and introduce the Hamiltonian for the process of Raman scattering. We derive the Heisenberg equations for atoms and photons and introduce the relevant correlation functions. In Sec. III, based on perturbative solution of the atomic dynamics, we calculate the one-body density matrix both in the position and momentum representations. In Sec. IV we discuss the method for incorporating the phase fluctuations due to the nonzero temperature of the quasicondensate. Then, we present the numerical results in two distinct cases. First, we describe the Raman scattering on a trapped quasicondensate. We calculate the density of scattered atoms both in the far-field regime and when the expansion of the halo of scattered atoms is short. Then, we turn to the second-order correlation function. We show how the temperature influences its peak height as well as the width. Finally, we demonstrate that when the Raman scattering is preceded by expansion of the quasicondensate, the density of scattered atoms widens while the second-order correlation function does not change substantially. Some details of calculations are presented in the Appendixes.

II. FORMULATION OF THE MODEL

The process of Raman scattering takes places when an atom in a three-level Λ configuration is illuminated with an intense pump beam. As a result of interaction with light, the atom absorbs a photon from the pump and undergoes an effective transition $0 \to 2 \to 1$ accompanied by spontaneous emission of a "Stokes" photon as shown in Fig. 1.

To model the phenomenon, we assume that the pump can be described classically as

$$E_p(\mathbf{r},t) = E_0(\mathbf{r},t)e^{i(\mathbf{k}_p\cdot\mathbf{r}-\omega_p t)} + \text{c.c.}, \tag{1}$$

where E_0 is its amplitude, $\mathbf{k}_p$ is the central wave vector, and $\omega_p = c|\mathbf{k}_p|$. When this frequency is strongly detuned from the transition $0 \to 2$, the upper level can be adiabatically

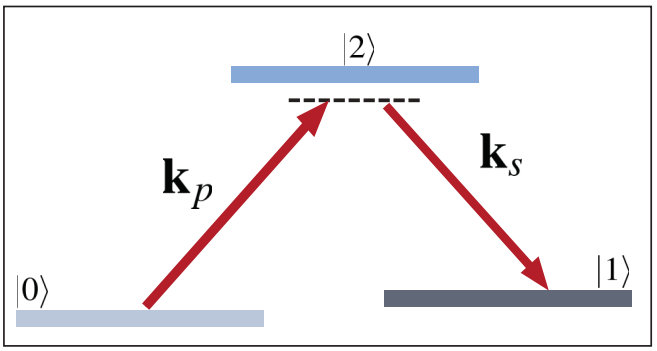

FIG. 1. (Color online) Scheme of atomic levels relevant in the process of Raman scattering. The atom, initially in state $|0\rangle$, absorbs strongly detuned pump photon with wave vector $\mathbf{k}_p$. The absorption is accompanied by spontaneous emission of a Stokes photon with wave vector $\mathbf{k}_s$. As a result, the atom undergoes a transition $0 \to 1$.

eliminated. The whole process can be regarded as creation of a quantum of atomic excitation $0 \to 1$ together with an emission of a Stokes photon.

We describe the quantum state of the atoms and Stokes photons using two field operators,

$$\hat{b}(\mathbf{k},t) = \frac{1}{\sqrt{N}} \sum_{\alpha} e^{i(\mathbf{k}\cdot\mathbf{r}_\alpha - \omega_{01}t)} |0\rangle_\alpha \langle 1|_\alpha, \tag{2}$$

$$\hat{E}_S^{(+)}(\mathbf{r},t) = \int d\mathbf{k}\, e^{i(\mathbf{k}\cdot\mathbf{r} - c|\mathbf{k}|t)} \hat{a}(\mathbf{k},t), \tag{3}$$

where ω_{01} is the $0 \to 1$ transition frequency. The operator $\hat{b}(\mathbf{k},t)$ annihilates an atomic excitation with momentum $\hbar\mathbf{k}$, while the index α runs over all the N atoms in the cloud. If the majority of atoms occupy $|0\rangle$, one can apply the Holstein-Primakoff approximation [41], and accordingly $\hat{b}$ satisfies bosonic commutation relations. Moreover, $\hat{E}_S^{(+)}$ is the field operator of the Stokes photons.

When a large number of atoms N occupy a single-particle state, one can replace summation over separate particles in Eq. (2) with an integral over the quasicondensate wave function $\psi(\mathbf{r},t)$. The effective Hamiltonian for the process of Raman scattering is $\hat{H} = \hat{H}_0 + \hat{H}_{\text{int}}$, where

$$\hat{H}_0 = \int d\mathbf{k}\, \hbar\omega_k \hat{a}^\dagger(\mathbf{k})\hat{a}(\mathbf{k}) + \int d\mathbf{k}\, \epsilon_k \hat{b}^\dagger(\mathbf{k})\hat{b}(\mathbf{k}) \tag{4}$$

is the free part, with $\epsilon_k = \hbar^2\mathbf{k}^2/2m$. Also, $\omega_k = c|\mathbf{k}| - \omega_S$ is centered around the Stokes frequency $\omega_S = \omega_p - \omega_{01}$.

The interaction Hamiltonian

$$\hat{H}_{\text{int}} = \int d\mathbf{k} d\mathbf{k}' h(\mathbf{k},\mathbf{k}')\, \hat{a}^\dagger(\mathbf{k},t)\hat{b}^\dagger(\mathbf{k}',t) + \text{H.c.} \tag{5}$$

governs the desired process, where an atomic excitation is created together with the Stokes photon. The coupling function $h(\mathbf{k},\mathbf{k}')$ is expressed in terms of a Fourier transform of the product of the quasicondensate and pump beam fields,

$$h(\mathbf{k},\mathbf{k}') = h_0 \int d\mathbf{r} e^{-i(\mathbf{k}+\mathbf{k}'-\mathbf{k}_p)\cdot\mathbf{r}} \psi(\mathbf{r},t) E_0(\mathbf{r},t), \tag{6}$$

where the coupling constant [42] is equal to

$$h_0 = \sqrt{\frac{\omega_s}{\hbar^{3/2}\varepsilon_0}} \frac{d_{02}d_{21}}{(2\pi)^3} \frac{2\omega_{02}}{\omega_{02}^2 - \omega_s^2}. \tag{7}$$

Here, d_{ij} is the atomic dipole moment associated with the $i \to j$ transition and ε_0 is the dielectric constant. Note that in Eq. (5) we have neglected the interaction of the scattered atoms with the mean field of the quasicondensate. This could have some impact on the Raman process, as discussed in detail in Sec. IV C.

Below we make further physically well-justified simplifications. First, we choose the pump envelope E_0 to be time independent, which corresponds to a common situation of square pulses. Moreover, the spatial extent of the pump usually vastly exceeds the size of the quasicondensate. Since the duration of the pump pulse is much shorter than the characteristic time scale of $\psi(\mathbf{r},t)$ dynamics, the quasicondensate wave function can be taken as constant, and the coupling function in a frame of reference moving with velocity $\hbar\mathbf{k}_p/m$ reads

$$h(\mathbf{k},\mathbf{k}') = h_0 E_0 \tilde{\psi}(\mathbf{k}+\mathbf{k}'). \tag{8}$$

Here, $\tilde{\psi}$ is a Fourier transform of wave function ψ.

We can now derive the set of coupled Heisenberg equations of motion for the Stokes and atomic field resulting from the Hamiltonian (4),

$$i\hbar\partial_t \hat{a}(\mathbf{k},t) = \hbar\omega_k \hat{a}(\mathbf{k},t) + \int d\mathbf{k}' h(\mathbf{k},\mathbf{k}')\hat{b}^\dagger(\mathbf{k}',t), \tag{9a}$$

$$i\hbar\partial_t \hat{b}(\mathbf{k},t) = \epsilon_k \hat{b}(\mathbf{k},t) + \int d\mathbf{k}' h(\mathbf{k}',\mathbf{k})\hat{a}^\dagger(\mathbf{k}',t). \tag{9b}$$

These equations are a starting point for the analysis of the second-order correlation function of scattered atoms, defined as

$$G^{(2)}(\mathbf{k}_1,\mathbf{k}_2,t) = \langle \hat{b}^\dagger(\mathbf{k}_1,t)\hat{b}^\dagger(\mathbf{k}_2,t)\hat{b}(\mathbf{k}_2,t)\hat{b}(\mathbf{k}_1,t)\rangle. \tag{10}$$

Since Eqs. (9) are linear and the initial state of scattered atoms and photons is a vacuum, then

$$G^{(2)}(\mathbf{k}_1,\mathbf{k}_2,t) = G^{(1)}(\mathbf{k}_1,\mathbf{k}_1,t)G^{(1)}(\mathbf{k}_2,\mathbf{k}_2,t) + |G^{(1)}(\mathbf{k}_1,\mathbf{k}_2,t)|^2 \tag{11}$$

is a function of the (one-body) density matrix, which reads

$$G^{(1)}(\mathbf{k}_1,\mathbf{k}_2,t) = \langle \hat{b}^\dagger(\mathbf{k}_1,t)\hat{b}(\mathbf{k}_2,t)\rangle. \tag{12}$$

Its diagonal part $n(\mathbf{k},t) = G^{(1)}(\mathbf{k},\mathbf{k},t)$ represents the momentum distribution of scattered atoms.

In the following section we derive analytical expressions for the density matrix in momentum and position representations, treating the atom-photon interactions in the perturbative manner.

III. PERTURBATIVE SOLUTIONS FOR ATOMS

When the number of scattered atom-photon pairs is small, one can solve Eq. (9b) perturbatively in the coupling constant h_0 defined in Eq. (7),

$$i\hbar\partial_t \hat{b}^{(1)}(\mathbf{k},t) = \epsilon_k \hat{b}^{(1)}(\mathbf{k},t) + \int d\mathbf{k}' h(\mathbf{k}',\mathbf{k})\hat{a}^\dagger(\mathbf{k}')e^{i\omega_{k'}t}, \tag{13}$$

where $\hat{a}^\dagger(\mathbf{k}') = \hat{a}^\dagger(\mathbf{k}',0)$. As we argue in Appendix A, since $\epsilon_k \ll \hbar\omega_k$, the first-order solution can be written as

$$\hat{b}^{(1)}(\mathbf{k},t) = e^{-i\frac{\epsilon_k t}{\hbar}}\hat{b}(\mathbf{k}) + \frac{te^{-i\frac{\epsilon_k t}{2\hbar}}}{i\hbar} \int d\mathbf{k}' h(\mathbf{k},\mathbf{k}')\hat{a}^\dagger(\mathbf{k}')\,\text{sinc}\left(\frac{\omega_{k'}t}{2}\right)e^{i\frac{\omega_{k'}t}{2}}. \tag{14}$$

This expression is used to calculate the first-order correlation function (12) of scattered atoms.

The measurement of positions of scattered atoms is performed as follows. First, the initial wave packet of the quasicondensate interacts with the pump beam for a time t_p and atoms scatter out of the mother cloud. Then, the system freely expands for a time t_f, and finally the positions of atoms are recorded. If t_f is sufficiently long and the system reaches the far-field regime, positions of atoms $\mathbf{r}_i$ are related to their wave vectors $\mathbf{k}_i$ by $\mathbf{k}_i = \frac{\mathbf{r}_i m}{\hbar t_f}$.

In the present work we compare the two possible experimental situations, when the system either is or is not in the far field. In the former case, as we argued above, it is sufficient to calculate the density matrix (12) in the momentum space just after the interaction ends. In the latter, we provide an expression for $G^{(1)}$ as a function of expansion time in position space.

A. Momentum-dependent density matrix

In order to calculate the momentum-dependent density matrix, note that for typical interaction times, the "sinc" function appearing in Eq. (14), which is peaked around $k' = k_s$, has much smaller width than the Fourier transform of the condensate function, which, via Eq. (8), enters $h(\mathbf{k},\mathbf{k}')$. Therefore, one can fix the length of the photon wave vector to be equal to k_s. Using the definition from Eq. (12) and the solution from Eq. (14) we obtain the density matrix in the momentum representation,

$$G^{(1)}(\mathbf{k}_1,\mathbf{k}_2) = \alpha \int d\Omega'\ \tilde{\psi}^{\star}(\mathbf{k}_1 + k_s\mathbf{n}')\tilde{\psi}(\mathbf{k}_2 + k_s\mathbf{n}'), \qquad (15)$$

where we omitted an irrelevant phase factor and $\alpha = \frac{2\pi t_p}{c\hbar^2}|h_0|^2|E_0|^2k_s^2$. The integration is performed over all the directions of the unit vector $\mathbf{n}'$. Since the above perturbative expression, apart from a trivial scaling of α with t_p, is time independent, we have skipped the time argument of $G^{(1)}$. All the intermediate steps leading to the above solution are presented in Appendix B. Finally, we emphasize that the momentum distribution of the scattered atoms could be broadened by the natural line width of the $2 \to 1$ transition. However, this effect is negligible compared to the momentum spread of the quasicondensate that enters Eq. (15).

By setting $\mathbf{k}_1 = \mathbf{k}_2 = \mathbf{k}$ we obtain the density of the scattered atoms

$$n(\mathbf{k}) = \alpha \int d\Omega\ |\tilde{\psi}(\mathbf{k} + k_s\mathbf{n})|^2, \qquad (16)$$

which is directly related to the momentum distribution of the quasicondensate. Integration over all directions of Stokes photon momentum $\mathbf{n}k_s$ is characteristic for a spontaneous regime, where photons scatter isotropically. Note also that since the quasicondensate wave function from Eq. (8) is expressed in the reference frame moving with the velocity $\hbar\mathbf{k}_p/m$, in the laboratory frame scattered atoms form a halo centered around $\mathbf{k}_p$ vector; see Fig. 2.

B. Position-dependent density matrix

To deal with situations when t_f is not sufficiently long for the system to enter the far-field regime, we provide an expression for the density matrix in position space as a function of the expansion time t_f, which up to an irrelevant phase factor reads

$$\tilde{G}^{(1)}(\mathbf{r}_1,\mathbf{r}_2,t_f) = \frac{\alpha}{(2\pi)^6}\int d\Omega\, S\left[\tilde{\psi}\left(\frac{\mathbf{r}_1 m}{\hbar t_f} + k_s\mathbf{n}\right)\right] S\left[\tilde{\psi}\left(\frac{\mathbf{r}_2 m}{\hbar t_f} + k_s\mathbf{n}\right)\right]^{\star}. \qquad (17)$$

Here, the functional S is given by

$$S[\tilde{\psi}(\mathbf{k})] = \int d(\delta\mathbf{k})\, e^{-i\frac{\hbar(\delta k)^2}{2m}t_f}\tilde{\psi}(\mathbf{k} + \delta\mathbf{k}). \qquad (18)$$

The derivation of Eq. (17) is presented in detail in Appendix C. Note that Eq. (17) resembles Eq. (15) except that $\tilde{\psi}$ is replaced with $S[\tilde{\psi}]$. The atomic density is obtained by setting $\mathbf{r}_1 = \mathbf{r}_2 = \mathbf{r}$ in Eq. (17) and reads

$$\tilde{n}(\mathbf{r},t_f) = \frac{\alpha}{(2\pi)^6}\int d\Omega \left| S\left[\tilde{\psi}\left(\frac{\mathbf{r}m}{\hbar t_f} + k_s\mathbf{n}\right)\right]\right|^2. \qquad (19)$$

We also emphasize that for sufficiently long t_f, $S[\tilde{\psi}(\mathbf{k})] \sim \tilde{\psi}(\mathbf{k})$, so the far field is reached.

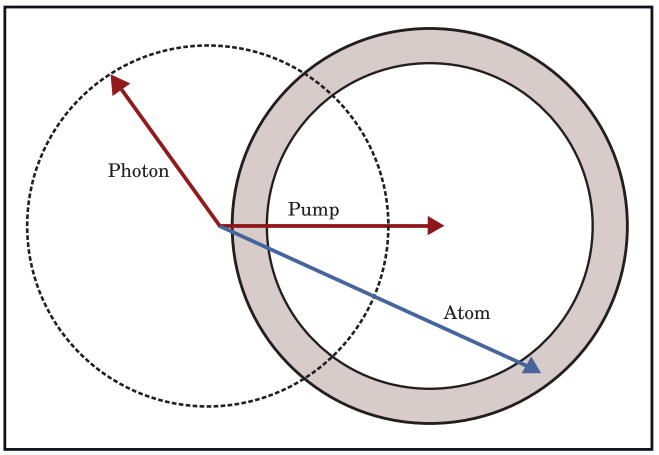

FIG. 2. (Color online) Scheme of the Raman scattering in the momentum space. Spontaneously emitted Stokes photon acquires momentum k_s. After many scattering events, the photons will form a sphere of radius k_s, denoted here by the dashed circle. Due to momentum conservation, atoms scatter onto a sphere of radius k_s as well, shifted by k_p due to absorption of the pump photon. The width of the gray ring occupied by the atoms represents the uncertainty resulting from the momentum spread of the parent quasicondensate.

IV. NUMERICAL RESULTS

In this section we calculate the correlation functions (15) and (17) using realistic experimental parameters. First, we briefly describe a numerical method for simulating phase fluctuations present in a strongly elongated ultracold bosonic gas.

A. Quasicondensate

We apply the above model to the process of Raman scattering of atoms from $N = 10^5$ metastable ^{4}He bosons with the atomic mass $m = 6.65 \times 10^{-27}$ kg and the scattering length

$a = 7.5 \times 10^{-9}$ m. The atoms are confined in a harmonic potential with the radial and the axial frequencies equal to $\omega_r = 2\pi \times 1500\,\frac{1}{\mathrm{s}}$ and $\omega_z = 2\pi \times 7.5\,\frac{1}{\mathrm{s}}$. Such an elongated gas is called a "quasicondensate" due to presence of the phase fluctuations along the z axis [37–39].

To account for the quasicondensate fluctuations, we use the method introduced in Refs. [37,38]. First, we evaluate numerically the density profile of the pure condensate by finding a ground state of the stationary Gross-Pitaevskii equation (GPE)

$$\mu\varphi(\mathbf{r}) = \left(-\frac{\hbar^2\nabla^2}{2m} + \frac{m\omega_r^2}{2}r^2 + \frac{m\omega_z^2}{2}z^2 + g|\varphi(\mathbf{r})|^2\right)\varphi(\mathbf{r}), \tag{20}$$

where $g = \frac{4\pi\hbar^2 a}{m}$ and $\mu = k_B \times 163\,\mathrm{nK}$ is the chemical potential.

Next, we construct the quasicondensate wave function $\psi(\mathbf{r})$ by imprinting a phase $\phi(z)$ onto the pure condensate function, $\psi(\mathbf{r}) = |\varphi(\mathbf{r})|e^{i\phi(z)}$, where

$$\phi(z) = \sum_{j=1}^{\infty}\sqrt{\frac{g\,\omega_r^2\,(j+2)(2j+3)}{4\pi\,z_{\mathrm{tf}}^3\,\omega_z^2\,\epsilon_j\,(j+1)}}\,P_j^{(1,1)}\left(\frac{z}{z_{\mathrm{tf}}}\right)\alpha_j. \tag{21}$$

Here, $\epsilon_j = \frac{\hbar\omega_z}{2}\sqrt{j(j+3)}$ is the energy of the low-lying axial excitations and $P_j^{(1,1)}$ is the Jacobi polynomial. Also, $z_{\mathrm{tf}} = 552\,\mu$m is the axial density width given by Thomas-Fermi approximation.

The phase fluctuations result from randomness of α_j, which is drawn from a Gaussian distribution with zero mean and the variance given by occupation of the jth mode

$$\langle\alpha_j^2\rangle = \frac{1}{\exp(\epsilon_j/k_BT) - 1}. \tag{22}$$

Consequently, the temperature of the gas enters the dynamics of the Raman scattering. Due to presence of the z-dependent phase factor (21) in the quasicondensate wave function, the momentum distribution along the z axis broadens as the temperature grows.

The quasicondensate is illuminated with an intense laser beam with the wave vector equal to $k_p = 5.80 \times 10^6\,m^{-1}$. Since the Stokes photon and the pump wave vectors are similar, we set $k_s \approx k_p$. Note that the length of the Stokes wave vector is the only relevant parameter of the pumping process that enters Eqs. (15) and (17). The other, like the pumping time t_p, the intensity of the laser, and its detuning from the $0 \to 2$ transition, defines the value of the coefficient α. In the perturbative regime, α is only a multiplicative factor, as can be seen from Eqs. (15) and (17), and thus has no physical importance for the shape of the functions considered here.

Our final simplification regards the form of the condensate density profile. A simple numerical check shows that the ground state of Eq. (20) can be approximated by a Gaussian function in the radial direction, so that

$$\psi(\mathbf{r}) = \sqrt{N\sigma_r^2}\pi e^{-\frac{\sigma_r^2}{2}(x^2+y^2)}\varphi(z)e^{i\phi(z)}. \tag{23}$$

The axial function $\varphi(z)$ is found numerically by setting $x = y = 0$ in Eq. (20) and the Gaussian fit gives $\sigma_r \simeq 0.10k_s$. All the numerical results presented below are obtained by calculating the relevant physical quantity for a single realization of the phase noise $\phi(z)$ and then averaging over many such realizations.

We can now estimate the free expansion time t_f, at which the system enters the far-field regime in the z direction. The velocity spread of the quasicondensate $\hbar\Delta k_z/m$ is approximately 2 mm/s, while the initial size is $2z_{\mathrm{tf}} \simeq 1$ mm. Therefore, the far-field condition would be $t_f \gg 2z_{\mathrm{tf}}/(\hbar\Delta k_z/m) = 0.5$ s.

Let us now comment on the consistency of the above approximations. Equation (21) was derived in Ref. [38] under the assumption that the quasicondensate has a Thomas-Fermi density profile in all three dimensions, valid when the nonlinear term dominates the Gross-Pitaevskii equation. To simplify our calculations, we model radial wave functions with Gaussian, which is true in the quasi-one-dimensional (quasi-1D) limit, when the radial trapping potential dominates over the nonlinear term. However, when we plot the numerically evaluated ground state of Eq. (20), it turns out to be in an intermediate regime, and could be equally well modeled with either a Gaussian or a Thomas-Fermi shape. Therefore, the above method can be regarded as an appropriate approach in such a transitional case. Since our main goal is to demonstrate the general behavior of the density and the correlation functions of scattered atoms as a function of T, we believe that this approximate method is sufficiently precise for the purpose.

B. Raman scattering on a trapped quasicondensate

In this section we present numerical results for the density and the second-order correlation function for the Raman scattering from a trapped quasicondensate. Although in this case a perturbative approach can be not very accurate, as discussed at the beginning of Sec. IV C, it is still a good starting point which allows us to grasp some basic properties of the halo of scattered atoms.

1. Density of scattered atoms

First, we present the numerical results for the momentum distribution of scattered atoms, as given by Eq. (16). We use the reference frame moving with a velocity $\hbar\mathbf{k}_p/m$, and hence according to Fig. 2 the density is centered around $\mathbf{k} = 0$ with the radius equal to k_s. We investigate the momentum density as a function of k_z in a vicinity of $\mathbf{k} = k_s\mathbf{e}_z$. This quantity, via Eq. (16), samples the z dependence of the momentum distribution of the quasicondensate and therefore may provide some information on its temperature.

In Fig. 3 we schematically show the main contribution to the density in Eq. (16) for $\mathbf{k} \simeq k_s\mathbf{e}_z$. When $k_z = k_s$, as in the main part of the figure, the integration runs approximately through the center of the cloud. When $k_z < k_s$, as in the inset (a), the tails of the quasicondensate still contribute to the density so the integral does not vanish rapidly as we move away from $k_z = k_s$. On the other hand, when $k_z > k_s$, shown in Fig. 3(b), the integral does not sample the tails anymore and the density of scattered atoms quickly drops with growing k_z.

This simple graphical interpretation is readily confirmed in Fig. 4, where we present the result of numerical integration of Eq. (16) with the quasicondensate function obtained for various temperatures and averaged over 400 realizations of the phase noise. As expected, for $T = 0.1$ nK the density is

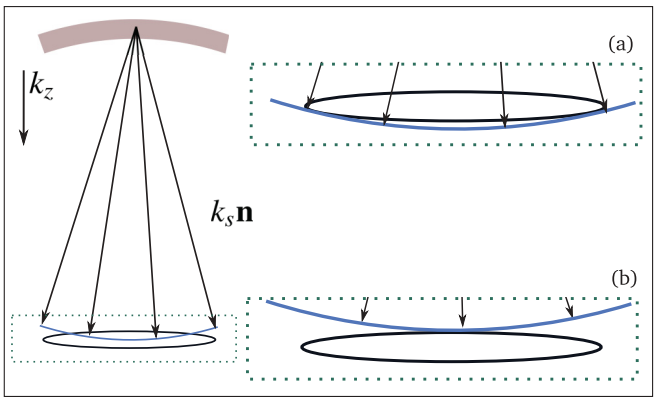

FIG. 3. (Color online) Graphical representation of the density integral (16) for $\mathbf{k} \simeq k_s\mathbf{e}_z$. The gray ring represents the halo of scattered atoms, in analogy to Fig. 2. When $\mathbf{k} = k_s\mathbf{e}_z$, as in the main part of the picture, the integration samples the majority of the atomic cloud, leading to value of the peak height. (a) When $|\mathbf{k}| < k_s$, the integration samples the tails of the quasicondensate and thus the density of scattered atoms does not vanish. (b) However, when $|\mathbf{k}| > k_s$, the tails do not contribute to the integral anymore and the density drops rapidly with growing k.

peaked around $k_z \simeq k_s$ and is largely extended for $k_z < k_s$, while it drops immediately as $k_z > k_s$. As the temperature grows, the density widens substantially due to increased width of the quasicondensate in the momentum space. Therefore, the density of scattered atoms, when measured along the k_z axis, could be used to determine the temperature of the mother cloud.

Next, we investigate the dependence of the atomic density measured in position space after a typical expansion time of $t_f = 300\,\mathrm{ms}$ [4–6]. At this time, as argued in the previous section, the system has not yet entered the far-field regime. We set $\frac{m\mathbf{r}}{\hbar t_f} \simeq k_s\mathbf{e}_\mathbf{z}$ in Eq. (19) to make a direct comparison with previous results and evaluate the integral numerically. We observe that when the expansion time is finite, contrary

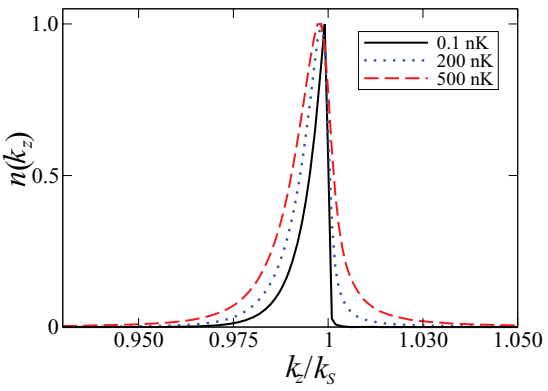

FIG. 4. (Color online) Density of scattered atoms for $\mathbf{k} \simeq k_s\mathbf{e}_\mathbf{z}$ for different temperatures and normalized by the value of the peak height. Each curve is an average over 400 realizations of the phase noise. The black solid line is calculated for the quasicondensate at $T = 0.1$ nK, the dotted blue (gray) line is for $T = 200$ nK, and the dashed red (gray) line is for $T = 500$ nK. The presence of the long tail for $k_z < k_s$, clearly visible for low temperatures, is graphically explained by insets of Fig. 3.

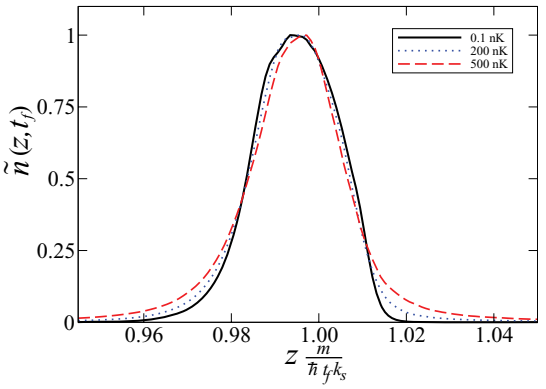

FIG. 5. (Color online) Density of scattered atoms for $\frac{m\mathbf{r}}{\hbar t_f} \simeq k_s\mathbf{e}_\mathbf{z}$ for different temperatures and normalized by the value of the peak height. The time of flight is $t_f = 300\,\mathrm{ms}$. Each curve is an average over 400 realizations of the phase noise. The black solid line is calculated for the quasicondensate at $T = 0.1$ nK, the dotted blue (gray) line is for $T = 200$ nK, and the dashed red (gray) line is for $T = 500$ nK.

to the far-field regime considered above, the density is less sensitive to the temperature, see Fig. 5. Also, we notice that for high T results in both cases are more similar. This is because at large temperatures, the momentum distribution of the quasicondensate broadens and so the far-field condition is satisfied at earlier times.

2. *Correlations between the scattered atoms*

We now investigate the impact of the phase fluctuations on the correlations of scattered atoms. We begin with the far-field expression (15) and using Eq. (11) we calculate the normalized second-order correlation function

$$g^{(2)}(\mathbf{k}_1,\mathbf{k}_2) = \frac{\langle G^{(2)}(\mathbf{k}_1,\mathbf{k}_2)\rangle_\phi}{\langle n(\mathbf{k}_1)\rangle_\phi \langle n(\mathbf{k}_2)\rangle_\phi}, \tag{24}$$

where $\langle\cdot\rangle_\phi$ denotes averaging over many realizations of the phase $\phi(z)$. In order to be consistent with the results of the previous section, we concentrate on a region of wave vectors close to $k_s\mathbf{e}_z$. Namely, we set $\mathbf{k}_1 = k_s\mathbf{e}_z + \frac{\Delta k}{2}\mathbf{e}_z$ and $\mathbf{k}_2 = k_s\mathbf{e}_z - \frac{\Delta k}{2}\mathbf{e}_z$ and analyze $g^{(2)}(\Delta k)$. First, note that for $\Delta k = 0$, according to Eq. (11) we have $g^{(2)}(0) = \frac{2\langle n^2\rangle_\phi}{\langle n\rangle_\phi^2}$, where $n = G^{(1)}(k_s\mathbf{e}_z, k_s\mathbf{e}_z)$. Since the variance $\langle n^2\rangle_\phi - \langle n\rangle_\phi^2$ is non-negative, then $g^{(2)}(0) \geqslant 2$. The inequality is saturated only in the absence of noise fluctuations. To picture the impact of the temperature on the height of the peak of the second-order correlation function, in Fig. 6 we plot $g^{(2)}(0)$ for various temperatures. We clearly notice the change of the height of the peak as soon as $T > 0$.

Next, in Fig. 7 we plot $g^{(2)}(\Delta k)$ as a function of Δk for various temperatures averaged for 400 realizations. We observe that apart from the change of the peak height $g^{(2)}(0)$, the wings of the correlation function broaden, due to increased momentum width of the quasicondensate at higher temperatures. When $T \simeq 0$, the correlation function oscillates in the momentum space. This behavior is determined by a Fourier transform of the Thomas-Fermi profile in the k_z

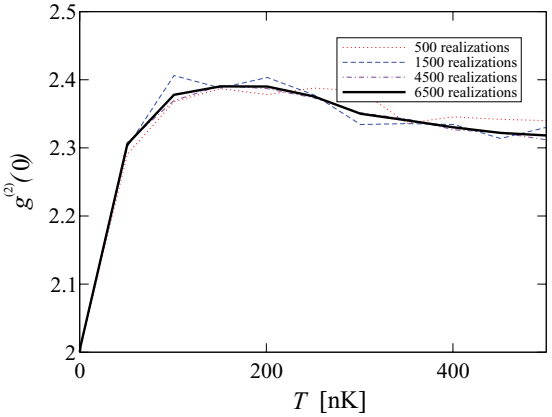

FIG. 6. (Color online) The peak of the second-order correlation function $g^{(2)}(0)$ as a function of temperature. Different curves correspond to averaging over various number of realizations. Clearly, $g^{(2)}(0) \geqslant 2$ and the inequality is saturated only for $T \simeq 0$.

direction. At larger temperatures, the phase fluctuations smear out the fringes.

We now switch to the finite expansion time regime and evaluate the normalized second-order correlation function in position space. Namely, we use the definition (11), where the $G^{(1)}$ function is calculated using Eq. (17), giving

$$\tilde{g}^{(2)}(\mathbf{r}_1,\mathbf{r}_2,t_f) = \frac{\langle G^{(2)}(\mathbf{r}_1,\mathbf{r}_2,t_f)\rangle_\phi}{\langle n(\mathbf{r}_1,t_f)\rangle_\phi \langle n(\mathbf{r}_2,t_f)\rangle_\phi}. \tag{25}$$

In analogy to the far-field case, we set $\mathbf{r}_1 = \frac{\hbar t_f}{m} k_s \mathbf{e}_z + \frac{\Delta z}{2}\mathbf{e}_z$ and $\mathbf{r}_2 = \frac{\hbar t_f}{m} k_s \mathbf{e}_z - \frac{\Delta z}{2}\mathbf{e}_z$. In Fig. 8 we plot $\tilde{g}^{(2)}(\Delta z,t_f)$ as a function of Δz for three different values of temperature T and $t_f = 300$ ms. Equivalently to the results obtained in the momentum space, we have $\tilde{g}^{(2)}(0,t_f) \geqslant 2$ and again we observe that this equality is saturated only for $T \simeq 0$. However, differently from the previous case, the oscillations of the correlation function at low temperatures are not present, since the Thomas-Fermi profile is a smooth function of z.

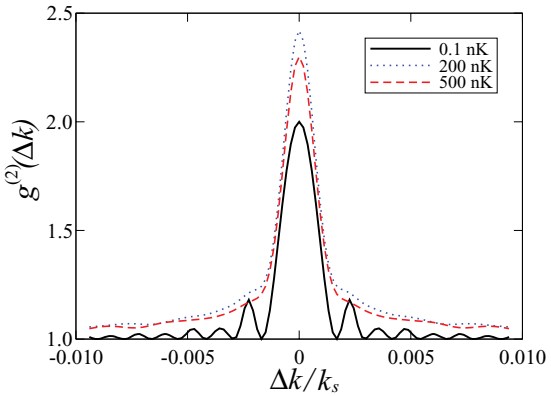

FIG. 7. (Color online) The dependence of the second-order correlation function $g^{(2)}(\Delta k)$ on the length of the wave vector Δk in a vicinity of $k_s\mathbf{e}_z$. The black solid line is calculated for $T = 0.1$ nK, the dotted blue (gray) line is for $T = 200$ nK, and the dashed red (gray) line is for $T = 500$ nK. The number of realizations was 400 for each curve.

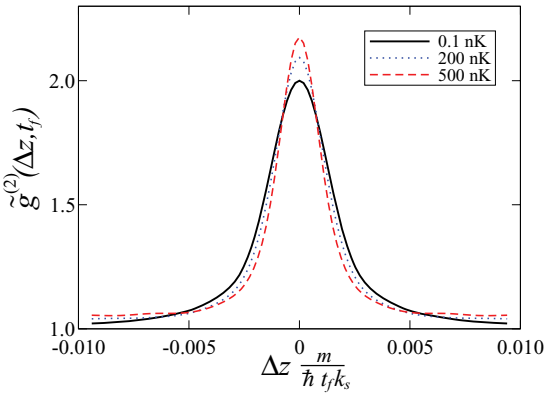

FIG. 8. (Color online) The dependence of the second-order correlation function $\tilde{g}^{(2)}(\Delta z,t_f)$ in the position space in a vicinity of $\frac{m\mathbf{r}}{\hbar t_f} = k_s\mathbf{e}_z$ as a function of Δz. The black solid line is calculated for $T = 0.1$ nK, the dotted blue (gray) line is for $T = 200$ nK, and the dashed red (gray) line is for $T = 500$ nK. The number of realizations was 400 for each curve.

Also, the broadening of the correlation function is much less pronounced.

C. Scattering on expanded quasicondensate

In the above considerations we have described Raman scattering from a quasicondensate just after its release from the trapping potential. In this case, if the pump pulse duration is sufficiently long and the mother cloud is strongly elongated in the z direction, we may observe an enhanced scattering into the "end-fire" modes along the z axis. This effect is related to bosonic enhancement and is not included in our perturbative description. The high aspect ratio of the quasicondensate we describe can lead to the stimulation effect even at very short illumination times when the number of scattered atoms is too small to be precisely measured. Additionally the cloud just after its release has a high peak density. When the scattered atoms propagate through such a dense medium, nonlinear potential can affect atomic trajectories, which is also not included in our model.

To avoid both difficulties described above we consider here the case when the quasicondensate expands considerably before Raman pulses are applied. During this expansion, the aspect ratio η of the axial-to-radial width decreases and so does the peak density; hence both bosonic stimulation and the mean-field repulsion of the scattered atoms can be safely neglected.

To estimate the expansion time which is sufficient to substantially reduce the density of the quasicondensate, we notice that after scattering away from the mother cloud, the atoms experience the mean-field potential equal to $2gn$, where n is the local density. As the scattered atoms leave the cloud, this potential is converted into the kinetic energy, and as a result their wave vector grows by $\Delta k \simeq \frac{2gn}{\hbar^2 k_s/m}$, which can be neglected as long as it is much smaller than the widths of the analyzed functions, which in case of $g^{(2)}$ is of the order of $10^{-3}k_s$; see Fig. 7. We have chosen the time of expansion time to be equal to 3 ms, so that the peak density drops by a factor of 800, which gives a negligible value of $\Delta k \simeq 10^{-4}k_s$.

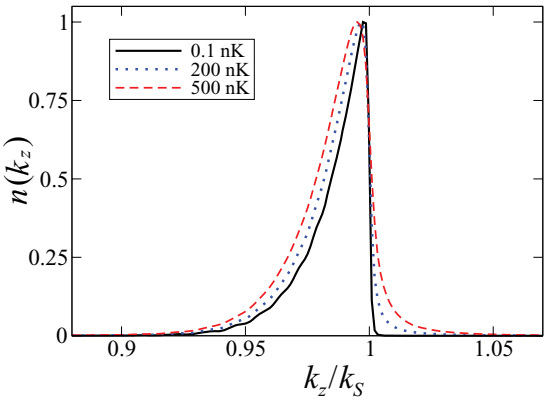

FIG. 9. (Color online) Density of scattered atoms for $\mathbf{k} \simeq k_s \mathbf{e_z}$ for different temperatures and normalized by the value of the peak height calculated with the quasicondensate after 3 ms of expansion. In analogy to Fig. 4, the black solid line is calculated for the quasicondensate at $T = 0.1$ nK, the dotted blue (gray) line is for $T = 200$ nK, and the dashed red (gray) line is for $T = 500$ nK.

Also, at this time the aspect ratio η drops from the value 125 to 3.7. However, it is a challenging task to directly propagate the quasicondensate wave function ψ for such a long time using the GPE, since it requires an extremely large spatial grid. Therefore, we employ an alternative scheme to generate ψ, which we use to calculate the one-body density matrix in the far field, as in Eq. (15). We describe in detail this numerical procedure in Appendix D.

1. Density of scattered atoms

In Fig. 9 we plot the density of scattered atoms as a function of k_z around the maximum localized at $k_z \simeq k_s$ for three different temperatures $T = 0.1$, 200, and 500 nK. The shape of the curves closely resembles the results presented in Fig. 4. However, the halo has clearly broadened, because the momentum width of the source increased substantially. To illustrate this effect, in Fig. 10 we compare the density calculated at $T = 200$ nK before and after the quasicondensate expansion. We notice that the broadening is present only in the tail, for $k_z < k_s$. It can be explained using the graphical

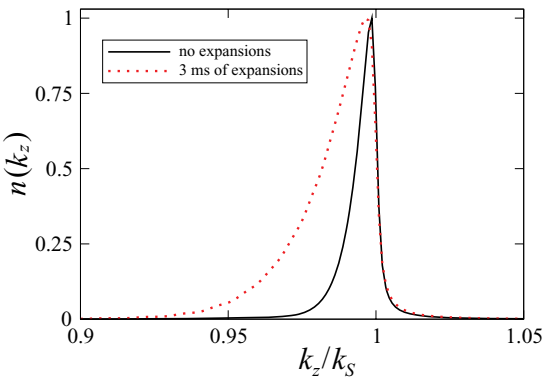

FIG. 10. (Color online) Comparison of the density of scattered atoms calculated with the quasicondensate just after the potential turn-off (solid black line) and after 3 ms of expansion (dotted red [gray] line). Both curves are calculated with 400 thermal trajectories at $T = 200$ nK.

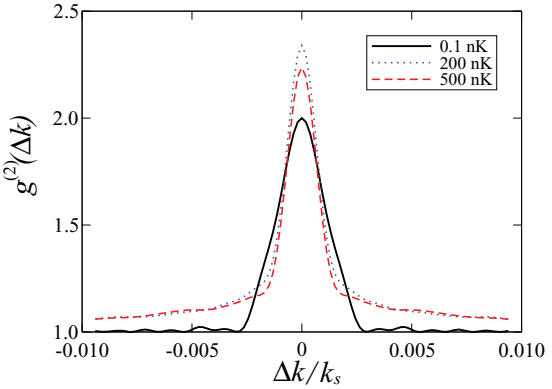

FIG. 11. (Color online) The $g^{(2)}(\Delta k)$ as a function of Δk in a vicinity of $k_s \mathbf{e}_z$ with a quasicondensate after 3 ms of expansion. The black solid line is calculated for $T = 0.1$ nK, the dotted blue (gray) line is for $T = 200$ nK, while the dashed red (gray) line is for $T = 500$ nK.

interpretation of the integral (15), which is presented in Fig. 3. As we argued before, the nonlinear expansion changes only the radial width of the quasicondensate momentum wave function. Figure 3 shows that the integral (15) for $k_z > k_s$ depends only on the axial density of the mother cloud and does not sample the radial wings. On the contrary, when $k_z < k_s$, the radial tails substantially contribute to the value of the integral and since the expansion mostly modifies these tails, we observe its effect only for $k_z < k_s$.

2. Correlations between the scattered atoms

Finally, in Fig. 11 we plot the normalized second-order correlation function (24) as a function of k_z for $T = 0.1$, 200, and 500 nK. Since the width of $g^{(2)}$ is related to the momentum width of the quasicondensate in the z direction—and this quantity is hardly influenced by the expansion—the second-order correlation function practically does not change as compared to Fig. 7.

To summarize this section, using the perturbative approach we have calculated the density and the second-order correlation function of scattered atoms when the Raman interaction is preceded by expansion of the quasicondensate to decrease the aspect ratio η and the peak density. These results, compared to scattering on a trapped cloud, show widening of the halo density and only minor modifications to $g^{(2)}$. However, the former results neglected the effect of bosonic enhancement and the impact of the mean field of the quasicondensate on the scattered atoms. This could have a significant impact on the Raman process, but inclusion of such phenomena is beyond the scope of this work.

We stress that stochastic numerical simulation of the whole dynamics, which would account for these effects, is impossible at the current technological level. This is because the scattered photons occupy an ultrathin halo of radius k_s and width $(ct)^{-1}$, where c is the speed of light and t is the interaction time. This width, even for an ultrashort interaction time $t = 1$ ns, is of the order of 10^{-6} k_s. To properly describe the Raman scattering, one would need to resolve the structure of this ultrathin halo, which is practically impossible.

V. CONCLUSIONS

We have analyzed the properties of the field of atoms scattered out of a quasicondensate in the Raman process. We have demonstrated that the density of scattered atoms, when measured in the far-field regime, depends on the temperature of the quasicondensate. However, this dependence is less pronounced when the expansion time is finite. Furthermore, we have calculated the second-order correlation function in both expansion time regimes. In each case, $g^{(2)}$ broadens with growing T, although in the latter the effect also is less evident. The temperature-induced phase fluctuations influence also the $g^{(2)}$ maximum. For the pure condensate, $g^{(2)}(0) = 2$ and grows at higher T.

We have also considered a situation when the Raman scattering is preceded by expansion of the mother cloud. We have shown that while the width of the scattering halo increases substantially, the second-order correlation function remains practically unchanged.

In summary, the measurements of the position of scattered atoms could provide some information on the temperature of the mother quasicondensate. Nevertheless, physical quantities such as the density or the correlation functions do not change substantially even within a wide range of temperatures $T \in [0,0.5]\,\mu$K. If the experiment is to be designed to identify the temperature of the quasicondensate, it must include a long free-expansion time t_f to reach the far-field regime. In our case, it is $t_f \geqslant 0.5s$. Also, high spatial resolution is required. For instance, from Fig. 4 we see that in order to distinguish the curves for $T = 200$ nK and $T = 500$ nK, one would need the momentum resolution $\Delta k_z \lesssim 0.025 k_s$. In order to estimate the spatial resolution Δx, we use the far-field relation $\Delta x = \Delta k_z \hbar t_f / m$. The experimental parameters used in this paper for $t_f = 0.5$ s, $\Delta x \lesssim 0.15$ mm would be necessary to discriminate the curves of different temperature.

Note that in our calculations we have neglected the possible impact of the atomic transition rules on the field of scattered atoms. In the case of particular atomic transitions, due to polarization of the Stokes field, some scattering directions are forbidden. We emphasize that such effect could be easily taken into account by modifying the coupling function $h(\mathbf{k}_1,\mathbf{k}_2)$.

ACKNOWLEDGMENTS

We are grateful to Wojciech Wasilewski, Marie Bonneau, Denis Boiron, and Chris Westbrook for fruitful discussions. T.W. acknowledges the Foundation for Polish Science International Ph.D. Projects Program cofinanced by the EU European Regional Development Fund. J. Ch. acknowledges Foundation for Polish Science International TEAM Program co-financed by the EU European Regional Development Fund and the support of the National Science Centre. P.Z. acknowledges the support of the Polish Ministry of Science and Higher Education program "Mobility Plus." M.T. acknowledges financial support of the National Science Centre.

APPENDIX A: PERTURBATIVE SOLUTION FOR THE ATOMS

In this Appendix we present details of the derivation of Eq. (14). First, we introduce a solution of Eq. (9a) in the absence of coupling, that is,

$$\hat{a}(\mathbf{k},t) = \hat{a}(\mathbf{k})e^{-i\omega_k t}. \tag{A1}$$

This expression, when inserted into Eq. (9b), gives a first-order equation of motion for the atomic field, which reads

$$\partial_t \hat{\beta}(\mathbf{k},t) = \frac{1}{i\hbar}\int d\mathbf{k}' h(\mathbf{k}',\mathbf{k})\hat{a}^\dagger(\mathbf{k}')e^{i(\omega_{k'}+\frac{\epsilon_k}{\hbar})t}, \tag{A2}$$

where $\hat{b}(\mathbf{k},t) = \hat{\beta}(\mathbf{k},t)e^{-i\epsilon_k t/\hbar}$. Integration over time gives

$$\hat{\beta}(\mathbf{k},t) = \hat{\beta}(\mathbf{k},0) + \frac{t}{i\hbar}\int d\mathbf{k}'\, h(\mathbf{k},\mathbf{k}')a^\dagger(\mathbf{k}') \times \operatorname{sinc}\left(\left(\omega_{k'} + \frac{\epsilon_k}{\hbar}\right)\frac{t}{2}\right)e^{i(\omega_{k'}+\frac{\epsilon_k}{\hbar})\frac{t}{2}}. \tag{A3}$$

The typical values of the kinetic energy of scattered atoms are $\epsilon_k \simeq \frac{\hbar^2 k_p^2}{2m}$, while the photon energies are of the order of $\omega_{k'} \simeq \hbar k_p c$. Since $mc/\hbar \sim 1.9 \times 10^{16} m^{-1}$ is of the order of the inverse of "Compton wavelength" of an atom, one can drop the dependence on the atom energy in the "sinc" function. We now express the above equation in terms of operator $\hat{b}$ and arrive at Eq. (14).

APPENDIX B: $G^{(1)}$ IN MOMENTUM SPACE

In this Appendix we derive Eq. (15). Using the perturbative solution from Eq. (14) and the definition of $G^{(1)}$ from Eq. (12), we obtain up to an irrelevant phase factor

$$G^{(1)}(\mathbf{k}_1,\mathbf{k}_2) = \frac{t_p^2}{\hbar^2}\int d\mathbf{k}' h^\star(\mathbf{k}_1,\mathbf{k}')h(\mathbf{k}_2,\mathbf{k}')\operatorname{sinc}^2\left(\frac{\omega_{k'}t_p}{2}\right). \tag{B1}$$

Typically the duration of the pump pulse is of the order of 5 μs. For such value, $\frac{1}{ct_p} \sim 1.5 \times 10^{-3}\,\frac{1}{m}$ is much smaller than the width of the coupling function h, which, via Eq. (8), is related to the Fourier transform of the quasicondensate function. Since $\omega_{k'}$ is centered around ω_s, we can set $|\mathbf{k}'| = k_s$ in the coupling function and perform the integral over k'. This way, we obtain

$$G^{(1)}(\mathbf{k}_1,\mathbf{k}_2) \simeq \frac{2\pi t_p k_s^2}{c\hbar^2}\int d\Omega\; h^*(\mathbf{k}_1,k_s\mathbf{n}')h(\mathbf{k}_2,k_s\mathbf{n}'), \tag{B2}$$

where $\mathbf{k}' = k_s\mathbf{n}'$, $|\mathbf{n}'| = 1$ and $\int d\Omega'$ denotes integration over a solid angle pointed by $\mathbf{n}'$. Using the definition of the coupling function from Eq. (8) we arrive at Eq. (15).

APPENDIX C: $G^{(1)}$ IN POSITION SPACE

In this appendix, we calculate the first-order correlation function in the position space after t_f time of the free expansion. We employ a reasonable approximation that the pump duration time t_p is much shorter than t_f. In this case, the position-dependent correlation function $\tilde{G}(\mathbf{k}_1,\mathbf{k}_2,t_f)$ is simply given by the following Fourier transform of Eq. (B2):

$$\tilde{G}^{(1)}(\mathbf{r}_1,\mathbf{r}_2,t_f) = \alpha\int d\Omega\; \Psi^*(\mathbf{r}_1,\mathbf{n},t_f)\Psi(\mathbf{r}_2,\mathbf{n},t_f), \tag{C1}$$

where $\alpha = \frac{2\pi t_p k_s^2}{c\hbar^2}|E_0|^2|h_0|^2$ and

$$\Psi(\mathbf{r},\mathbf{n},t_f) = \int\frac{d\mathbf{k}}{(2\pi)^3}\, e^{-i\frac{\epsilon_k t_f}{\hbar}+i\mathbf{k}\cdot\mathbf{r}}\tilde{\psi}(\mathbf{k}+k_s\mathbf{n}). \tag{C2}$$

Changing the variables to $\mathbf{k} = \frac{m\mathbf{r}}{\hbar t_f} + \delta\mathbf{k}$ gives Eq. (17), up to an irrelevant phase factor.

APPENDIX D: CALCULATING WAVE FUNCTION AFTER EXPANSION

As we mentioned in the main text, it is virtually impossible to calculate ψ after 3 ms of expansion by simply running GP numerically. In this appendix we present the details of the approximate method of generating a quasicondensate wave function that captures all the important features of the expansion dynamics.

Our approach is based on the observation that the nonlinearity is important only at the early stage of the expansion, when it modifies the Fourier transform $\tilde{\psi}$ of the wave function. Afterward, in the linear regime, $\tilde{\psi}$ gains the time-dependent phase, but its shape remains unaltered. We run the numerical simulation of the free GPE on a dense spatial grid until $t_{\mathrm{ex}}^{(1)} = 0.5$ ms, when the peak density drops by a factor of 22 and the nonlinearity does not count any more. From now on, we use a free Schrödinger equation to propagate ψ until $t_{\mathrm{ex}} = 3$ ms. To this end, we numerically calculate the Fourier transform and get $\tilde{\psi}(\mathbf{k}, t_{\mathrm{ex}}^{(1)})$. Since the grid in the position space was very dense, the wave vectors $\mathbf{k}$ are not very well resolved. Therefore, using the function itself together with its first momentum derivative, we interpolate $\tilde{\psi}$, which vastly improves the precision of the numerical method. The interpolated $\tilde{\psi}$ is then expanded analytically from $t_{\mathrm{ex}}^{(1)} = 0.5$ ms to $t_{\mathrm{ex}}^{(1)} = 3$ ms with the free propagator. This way, we obtain the wave function $\tilde{\psi}(\mathbf{k}, t_{\mathrm{ex}})$, which we use to calculate the far-field density matrix as in Eq. (15). The procedure is repeated 400 times to average the result over many thermal trajectories.

[1] Wim Vassen, Claude Cohen-Tannoudji, Michele Leduc, Denis Boiron, Christoph I. Westbrook, Andrew Truscott, Ken Baldwin, Gerhard Birkl, Pablo Cancio, and Marek Trippenbach, Rev. Mod. Phys. **84**, 175 (2012).

[2] M. Kozuma, L. Deng, E. W. Hagley, J. Wen, R. Lutwak, K. Helmerson, S. L. Rolston, and W. D. Phillips, Phys. Rev. Lett. **82**, 871 (1999).

[3] J. M. Vogels, K. Xu, and W. Ketterle, Phys. Rev. Lett. **89**, 020401 (2002).

[4] A. Perrin, H. Chang, V. Krachmalnicoff, M. Schellekens, D. Boiron, A. Aspect, and C. I. Westbrook, Phys. Rev. Lett. **99**, 150405 (2007).

[5] V. Krachmalnicoff, J.-C. Jaskula, M. Bonneau, V. Leung, G. B. Partridge, D. Boiron, C. I. Westbrook, P. Deuar, P. Zi, M. Trippenbach, and K. V. Kheruntsyan, Phys. Rev. Lett. **104**, 150402 (2010).

[6] J.-C. Jaskula, M. Bonneau, G. B. Partridge, V. Krachmalnicoff, P. Deuar, K. V. Kheruntsyan, A. Aspect, D. Boiron, and C. I. Westbrook, Phys. Rev. Lett. **105**, 190402 (2010).

[7] W. RuGway, S. S. Hodgman, R. G. Dall, M. T. Johnsson, and A. G. Truscott, Phys. Rev. Lett. **107**, 075301 (2011).

[8] R. A. Williams, L. J. LeBlanc, K. Jiménez-García, M. C. Beeler, A. R. Perry, W. D. Phillips, and I. B. Spielman, Science **335**, 314 (2012).

[9] R. Bach, M. Trippenbach, and K. Rzążewski, Phys. Rev. A **65**, 063605 (2002).

[10] P. Ziń, J. Chwedeńczuk, A. Veitia, K. Rzążewski, and M. Trippenbach, Phys. Rev. Lett. **94**, 200401 (2005).

[11] P. Ziń, J. Chwedeńczuk, and M. Trippenbach, Phys. Rev. A **73**, 033602 (2006).

[12] J. Chwedeńczuk, P. Ziń, K. Rzążewski, and M. Trippenbach, Phys. Rev. Lett. **97**, 170404 (2006).

[13] J. Chwedeńczuk, P. Ziń, M. Trippenbach, A. Perrin, V. Leung, D. Boiron, and C. I. Westbrook, Phys. Rev. A **78**, 053605 (2008).

[14] A. A. Norrie, R. J. Ballagh, and C. W. Gardiner, Phys. Rev. Lett. **94**, 040401 (2005).

[15] P. Deuar and P. D. Drummond, Phys. Rev. Lett. **98**, 120402 (2007).

[16] P. Deuar, Phys. Rev. Lett. **103**, 130402 (2009).

[17] P. Deuar, J. Chwedeńczuk, M. Trippenbach, and P. Ziń, Phys. Rev. A **83**, 063625 (2011).

[18] P. Deuar, P. Ziń, J. Chwedeńczuk, and M. Trippenbach, Eur. Phys. J. D **65**, 19 (2011).

[19] A. D. Cronin, J. Schmiedmayer, and D. E. Pritchard, Rev. Mod. Phys. **81**, 1051 (2009), and references therein

[20] C. Klempt, O. Topic, G. Gebreyesus, M. Scherer, T. Henninger, P. Hyllus, W. Ertmer, L. Santos, and J. J. Arlt, Phys. Rev. Lett. **103**, 195302 (2009).

[21] C. Klempt, O. Topic, G. Gebreyesus, M. Scherer, T. Henninger, P. Hyllus, W. Ertmer, L. Santos, and J. J. Arlt, Phys. Rev. Lett. **104**, 195303 (2010).

[22] B. Lücke, M. Scherer, J. Kruse, L. Pezzé, F. Deuretzbacher, P. Hyllus, O. Topic, J. Peise, W. Ertmer, J. Arlt, L. Santos, A. Smerzi, and C. Klempt, Science **334**, 773 (2011).

[23] K. Hammerer, A. S. Sørensen, and E. S. Polzik, Rev. Mod. Phys. **82**, 1041 (2010).

[24] C. Simon *et al.*, Eur. Phys. J. D **58**, 1 (2010).

[25] S. Inouye, A. P. Chikkatur, D. M. Stamper-Kurn, J. Stenger, D. E. Pritchard, and W. Ketterle, Science **285**, 571 (1999).

[26] J. Stenger, S. Inouye, D. M. Stamper-Kurn, A. P. Chikkatur, D. E. Pritchard, and W. Ketterle, Appl. Phys. B **69**, 347 (1999).

[27] M. G. Moore and P. Meystre, Phys. Rev. Lett. **85**, 5026 (2000).

[28] M. G. Payne and L. Deng, Phys. Rev. A **64**, 031802(R) (2001).

[29] X. Xu, X. Zhou, and X. Chen, Phys. Rev. A **79**, 033605 (2009).

[30] T. Wang and S. F. Yelin, Phys. Rev. A **72**, 043804 (2005).

[31] H. Uys and P. Meystre, Phys. Rev. A **77**, 063614 (2008).

[32] Y. Yoshikawa, Y. Torii, and T. Kuga, Phys. Rev. Lett. **94**, 083602 (2005).

[33] D. Schneble, G. K. Campbell, E. W. Streed, M. Boyd, D. E. Pritchard, and W. Ketterle, Phys. Rev. A **69**, 041601(R) (2004).

[34] Y. Yoshikawa, T. Sugiura, Y. Torii, and T. Kuga, Phys. Rev. A **69**, 041603(R) (2004).

[35] Y. Yoshikawa, K. Nakayama, Y. Torii, and T. Kuga, Phys. Rev. Lett. **99**, 220407 (2007).

[36] L. E. Sadler, J. M. Higbie, S. R. Leslie, M. Vengalattore, and D. M. Stamper-Kurn, Phys. Rev. Lett. **98**, 110401 (2007).

[37] S. Dettmer *et al.*, Phys. Rev. Lett. **87**, 160406 (2001).
[38] D. S. Petrov, G. V. Shlyapnikov, and J. T. M. Walraven, Phys. Rev. Lett. **87**, 050404 (2001).
[39] D. S. Petrov, D. M. Gangardt, and G. V. Shlyapnikov, J. Phys. IV France **116**, 3 (2004).
[40] S. Richard, F. Gerbier, J. H. Thywissen, M. Hugbart, P. Bouyer, and A. Aspect, Phys. Rev. Lett. **91**, 010405 (2003).
[41] T. Holstein and H. Primakoff, Phys. Rev. **58**, 1098 (1940).
[42] M. G. Raymer, I. A. Walmsley, J. Mostowski, and B. Sobolewska, Phys. Rev. A **32**, 332 (1985).